ELSEVIER

European Journal of Mechanics B/Fluids 21 (2002) 383–398

EUROPEAN JOURNAL OF MECHANICS B/FLUIDS

Buoyant flow in long vertical enclosures in the presence of a strong horizontal magnetic field. Part 1. Fully-established flow

Toshio Tagawa [b], Guillaume Authié [a,*], René Moreau [a]

[a] *Laboratoire EPM-Madylam, UPR CNRS A 9033, ENSHMG, BP 95, 38402 Saint-Martin d'Hères cedex, France*
[b] *Visitor from Institute of Advanced Material Study, Kyushu University, 6-1, Kasuga-koen, Kasuga 816-8583, Japan*

Received 6 September 2000; received in revised form 17 December 2001; accepted 11 January 2002

Abstract

The buoyant convection in a long vertical rectangular enclosure under the presence of a horizontal uniform magnetic field is investigated. Two opposite vertical walls are kept at different temperatures and the other four walls are thermally insulating. The main parameters of this study are the Grashoff number Gr, and the Hartmann number Ha. The applied magnetic field is either perpendicular or parallel to the temperature gradient. In both configurations, if it is large enough, it damps out the buoyant flow and ensures a conductive heat flux, but with different scaling laws: Gr/Ha for the perpendicular case, $\mathrm{Gr}/\mathrm{Ha}^2$ for the parallel case. This first paper focuses on the fully-established flow, far from the top and the bottom of the enclosure, in the limit of high Ha. Analytical solutions are derived and serve as reference to validate the numerical results. An analytical model of the Hartmann layers describes directly their influence on the core flow, saves important computational resources and yields quite accurate results.

Keywords: Magnetohydrodynamics; Convection; Hartmann layers; Side layers; Thermonuclear fusion

1. Introduction

In one of the concepts of the liquid metal blanket for the nuclear fusion reactor, the liquid metal (Li–Pb in the European program) flows at a very low velocity (a few mm/s), such that the flow rate is sufficient to remove the tritium produced within the fluid volume by the breeding reaction. Conduction is sufficient to transfer the heat generated by this reaction to water-cooled tubes whose shape and position are not yet fixed. The whole blanket is divided into a large number of very long ducts (length of the order of 10 m), almost vertical and whose cross-section is close to a square of typical side length $l \sim 15$ cm separated by thin metallic walls, in which the water-cooled tubes are located. Some natural convection takes place in the presence of the horizontal temperature gradient. Although it is braked by the strong toroidal magnetic field (up to 10 Tesla) necessary to confine the plasma, large convective velocities are expected within the liquid metal. Since they result from a balance between buoyancy and Lorentz force, they may scale between $\mathrm{Gr}/\mathrm{Ha}^2$ and Gr/Ha (Gr and Ha denote the Grashoff and Hartmann numbers) depending on the directions of the magnetic field B and of the temperature gradient, on the electrical conductivities of the walls, and on the symmetries (see Alboussière et al. [1]). They may reach values of the order of a few dozens of cm/s to 1 m/s. They are so large in comparison with the mean velocity that, in a first approximation, the mean flow may be neglected, and the emphasis may be focused on the pure buoyant flow. From previous studies in different geometries, one may expect that the stabilizing influence of the magnetic field is sufficient to damp all kinds of disturbances and lead to a laminar regime, but this particular point is going to be checked in a mercury experiment (to be presented in a companion paper, Part 2). It seems to be a necessary first step to investigate this kind of MHD buoyant flow in a simple geometry, such as an infinitely long enclosure with

* Correspondence and reprints.
E-mail address: guillaum@hmg.inpg.fr (G. Authié).

0997-7546/02/$ – see front matter
PII: S0997-7546(02)01182-2

a square cross-section, neglecting the electrical coupling between the different channels. The flow should be organized with a core, recirculation zones at the top and the bottom of the enclosure, and thin viscous boundary layers. With the characteristics mentioned above ($l = 15$ cm, $B = 10$ T), the Hartmann number reaches 10^4, the Hartmann layers along the walls perpendicular to B extend over a thickness $O(l \cdot Ha^{-1})$ of a few microns, and the side layers along the walls parallel to B have a thickness $O(l \cdot Ha^{-1/2})$ smaller than one millimetre.

The purpose of this paper is to present both the analytical solutions for such a flow in the approximation of a fully-established regime and a well validated numerical tool to compute the actual flow. The equilibrium between buoyancy and pressure forces in the end regions shows (see Part 2) that they extend over a typical length of the same order as the side of the section and do not have any effect on the long fully-established domain. In addition, in the actual blanket design, the shape of these top and bottom parts, where the fluid enters and exits, is still not determined. This approximation has two major consequences:

(i) the flow is parallel to the vertical axis, and
(ii) the heat transfer from one wall to the other, or from the volumetric source to the cooled walls, is purely conductive, so that the Prandtl number is not relevant and the temperature distribution is independent of the flow.

As indicated by Walker and Picologlou [14] for pressure-driven flows in a similar range of Ha numbers, the numerical modelling of the Hartmann layers, where the velocity and current density distributions have simple exponential dependences, is just "a waste of the computational resources." But, because the electric current density can be Ha times larger within these layers than within the core, it is essential to model them with enough accuracy to satisfy the global conservation of the electric current. If this is done numerically, it requires a significant number of mesh points within the layer and, as a consequence, extremely large computational resources (memory and CPU time). When it is done analytically, it saves the computational resources, but the lowest limit of the Hartmann number above which this analytical modeling is correct is still not clear. It is therefore also one of the aims of this paper to compare both numerical approaches for Ha numbers larger than 100 with the analytical results in order to develop guidelines for those who may intend to compute such flows. We primarily apply these guidelines in the companion paper (Part 2. Finite vertical enclosures) where the entire 3D flow, which can be reduced to a 2D flow for large Hartmann numbers, is also computed.

The next section presents the formulation of the problem. Although they have been known since Hunt and Ludford, (1968) [4], the properties of the Hartmann layers are summarized and the boundary conditions for the core flow at the Hartmann walls are briefly derived. Since the Hartmann walls are parallel to each other and the magnetic field is uniform, this derivation and their expressions are simpler than in the papers on flows in non-uniform magnetic fields [8,13], or on flows in ducts of varying cross-section [14]. Then, Section 3 presents analytical asymptotic solutions for MHD buoyant flows in such square enclosures. These solutions reveal the influence of the Hartmann layers on the velocity distributions in both the core and the side layers. And in Section 4, we present the numerical results which were obtained in the same geometry and we compare them with the analytical solution.

2. Model system and governing equations

In the entire paper we assume that $Ha \gg 1$ and Gr/Ha is moderate. The asymptotic modelling of the Hartmann layers at the first order in Ha^{-1}, is made in the general case of a thick wall of arbitrary conductivity. Then, the method to solve the fully-established flow is given for insulating walls, for any temperature distribution, and for any flow rate. Nevertheless, we apply it for thermal conductive cases with no volumetric heat source, so that the temperature profile is linear between hot and cold walls, and for natural convection in a closed enclosure, so that the flow rate is zero.

2.1. Governing equations

The problem to be considered is illustrated on Fig. 1. A liquid metal is enclosed in a vertically elongated cavity with a square cross-section. It is heated from one vertical wall at a given temperature (Th) and cooled by the opposite wall also at a given temperature (Tc). The two other walls are thermally insulating. A horizontal uniform magnetic field, either *perpendicular* or *parallel* to the heat flux, is applied in the (Oy) direction. We denote the width of each wall as l so that $Y = y/l$, $X = x/l$ are the dimensionless coordinates. Since the vertical flow is assumed to be fully-established, the purely conductive temperature distribution in dimensionless notation is either $\theta = 1/2 - Y$ in the "*parallel*" case, or $\theta = 1/2 - X$ in the "*perpendicular*" case, where $\theta = [T - 1/2(T_h + T_c)]/(T_h - T_c)$ is the dimensionless temperature.

The main quantities of interest (velocity, current density components and electric potential) are independent of the z coordinate and are defined within the square cross section shown in Fig. 2. They are governed by the following dimensionless equations (momentum equation, Ohm's law and electric charge conservation),

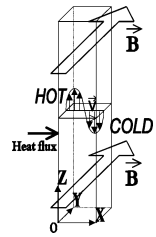

Fig. 1. Schematic of the enclosure with an applied magnetic field *perpendicular* to the heat flux.

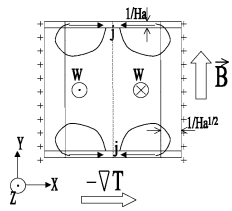

Fig. 2. Main phenomena in a fully established flow for the *perpendicular* case.

$$\Delta W + \mathrm{Ha}^2 J_x + \mathrm{Gr}\theta = 0, \tag{1}$$

$$J_x = -\frac{\partial \Phi}{\partial X} - W, \quad J_y = -\frac{\partial \Phi}{\partial Y}, \tag{2}$$

$$\frac{\partial J_x}{\partial X} + \frac{\partial J_y}{\partial Y} = 0, \tag{3}$$

where W is the vertical velocity normalized by ν/l, J_x and J_y are the component of the electric current density normalized by $\nu\sigma B/l$, Φ is the electric potential function normalized by νB, $\mathrm{Ha} = \sqrt{\sigma/\rho\nu}Bl$ is the Hartmann number and $\mathrm{Gr} = g\beta(T_h - T_c)l^3/\nu^2$ is the Grashoff number, while ρ, ν, β and σ are the density, kinematic viscosity, volumetric expansion coefficient and electrical conductivity of the liquid metal.

For the particular case of this fully-established flow, it would be possible to use a different characteristic velocity ($\nu/l \times \mathrm{Gr}/\mathrm{Ha}^2$), so that only one parameter Ha would remain. However, in order to make easier the comparison with the case of a recirculating flow in a finite-height enclosure, to be presented in the companion paper (Part 2), we prefer to keep Gr as an explicit parameter.

The boundary conditions are the no-slip condition ($W = 0$) at the walls ($X = 0, 1$ and $Y = 0, 1$) and the continuity of the component of the current density normal to the walls ($J_x = 0$ at $X = 0, 1$, and $J_y = 0$ at $Y = 0, 1$ for insulating walls). In principle, this continuity is valid for any electrical conductivity σ_w and thickness e of the wall. But, except in the derivation of the boundary conditions for the core flow at the Hartmann walls (where a non zero conductivity of the wall is taken into account), we limit ourselves to the simple case of insulating walls ($\vec{J} \cdot \vec{n} = 0$).

2.2. Modelling of the Hartmann layers and boundary conditions for the core flow

Let us now consider the properties of the Hartmann layers, which were first derived by Hunt and Ludford [4] for flows without inertia or buoyancy, and which have been reviewed by Hunt and Shercliff [5]. Under conditions such that the interaction parameter is much larger than unity, inertia is negligible compared to the viscous friction and Lorentz force, whose balance is the predominant feature within the Hartmann layer. It has been demonstrated by Sommeria and Moreau [10] that, even in the presence of turbulence within the core flow, those properties are still valid (see also Moreau [7, p. 126–131 and 293–296]). In the case of pressure-driven duct flows, they have been reexamined by Walker and his co-workers in several papers [8,13,14]. And Bülher [2] gives a solution for the buoyant flow with a series expansion for the side layers. In the following, we just intend to summarize these properties and to derive from them the boundary conditions which have to be satisfied by the core flow at the Hartmann walls. The quite minor changes due to buoyancy are mentioned.

In this section, the superscript (^{0}) denotes to quantities within the core, whereas the same symbol without any superscript denotes its value within the Hartmann layer. The unit vector in the direction of the magnetic field is $\vec{y}$, and the distance to any Hartmann wall is denoted as N ($N = Y$ or $1 - Y$). The velocity is decomposed in both components $\vec{U}_{//}$ and $\vec{U}_{\perp}$, parallel and perpendicular to $\vec{n}$.

A well known property of pressure driven flows at large Ha is the fact that, within the core, the second derivative of the electric potential in the magnetic field direction is zero. This is not true when a body force varying in the direction perpendicular to the magnetic field is present. In the presence of buoyancy the appropriate core equation is

$$\frac{\partial^2 \Phi^0}{\partial Y^2} = \frac{\mathrm{Gr}}{\mathrm{Ha}^2}\left(\vec{g} \times \vec{\nabla}\theta^0\right) \cdot \vec{y}. \tag{4}$$

If $\vec{g} = -\vec{z}$ (vertical channel), it becomes

$$\frac{\partial^2 \Phi^0}{\partial Y^2} = -\frac{\mathrm{Gr}}{\mathrm{Ha}^2}\frac{\partial \theta^0}{\partial X}. \tag{5}$$

This expression (4) shows that, when the three vectors on the right-hand side are orthogonal to each other (the *perpendicular* case), the MHD equivalent of the Taylor–Proudman theorem applies within the core. But within the Hartmann layer this second derivative may be derived from an expression which is the difference between the expressions within the layer and within the core:

$$\frac{\partial^2 \Phi}{\partial Y^2} + \Delta\left(\Phi - \Phi^0\right) = \left[\vec{\nabla}_\perp \times \left(\vec{U}_\perp - \vec{U}_\perp^0\right)\right] \cdot \vec{y} + \frac{\mathrm{Gr}}{\mathrm{Ha}^2}\left(\vec{g} \times \vec{\nabla}\theta^0\right) \cdot \vec{y}. \tag{6}$$

It appears that the variation of the electric potential due to buoyancy over the thickness of the Hartmann layer ($\mathrm{O}(\mathrm{Ha}^{-1})$) would be of the order of $\mathrm{Gr}/\mathrm{Ha}^4$. Even if $\mathrm{Gr}/\mathrm{Ha}^2$ may be of order unity, we assume that $\mathrm{Gr}/\mathrm{Ha}^4$ is much smaller than unity and, therefore, that the electric potential has a negligible variation across the Hartmann layer. And from similar arguments, as in ordinary flows, it may be shown that temperature and pressure do not vary across the Hartmann layer.

Then the projection of the momentum equation onto the plane perpendicular to the magnetic field is:

$$\frac{\mathrm{d}\vec{U}_\perp}{\mathrm{d}t} + \vec{\nabla}_\perp P = -\mathrm{Gr} \cdot \theta \cdot \vec{g}_\perp - \mathrm{Ha}^2\left(\vec{\nabla}_\perp \Phi \times \vec{y} + \vec{U}_\perp\right) + \frac{\partial^2 \vec{U}_\perp}{\partial Y^2}. \tag{7}$$

Substracting this equation from the same one written in the core flow yields the classical equation for the velocity distribution within the Hartmann layer

$$\frac{\partial^2 \vec{U}_\perp}{\partial N^2} - \mathrm{Ha}^2\left(\vec{U}_\perp - \vec{U}_\perp^0\right) = 0, \tag{8}$$

whose solution satisfying the no-slip condition at the wall and matching the core velocity is the usual exponential profile

$$\vec{U}_\perp = \vec{U}_\perp^0 - \left[\vec{U}_\perp^0\right]_{N=0} \cdot \mathrm{e}^{-\mathrm{Ha}N}. \tag{9}$$

It is therefore clear that, for these asymptotic conditions, even in the presence of inertia and buoyancy, this profile is unchanged. Notice that the components of the core velocity in the vicinity of the Hartmann layer cannot have a significant variation in the magnetic field direction. In other words,

$$\left[\frac{\partial \vec{U}_\perp^0}{\partial N}\right]_{N=0} \sim \frac{1}{\mathrm{Ha}}\left[\frac{\partial \vec{U}_\perp}{\partial N}\right]_{N=0} \approx 0. \tag{10}$$

Two important properties of the Hartmann layer, which will be used as boundary conditions for the core flow in our numerical analysis, may be derived from the integration of the mass and electric charge conservation equations across the Hartmann layer. The first one, which results from the continuity equation $\partial(U_{/\!/} - U_{/\!/}^0)/\partial N + \vec{\nabla}_\perp \cdot (\vec{U}_\perp - \vec{U}_\perp^0) = 0$, yields

$$\left[U_{/\!/}^0\right]_{N=0} = \frac{1}{\mathrm{Ha}}\left[\vec{\nabla}_\perp \cdot \vec{U}_\perp^0\right]_{N=0}. \tag{11}$$

Since the velocity is of order unity, $\vec{U}_\perp^0$ is of order unity within this layer, this condition reduces to $[U_{/\!/}^0]_{N=0} = 0$ in the limit of large Ha numbers.

And the second one result from the conservation of the electric current. Substituting (9) in Ohm's law gives

$$\vec{J}_\perp = \vec{J}_\perp^{\,0} - \left(\left[\vec{U}_\perp^0\right]_{N=0} \times \vec{y}\right) \cdot \mathrm{e}^{-\mathrm{Ha}N}. \tag{12}$$

Then, integrating the difference $\vec{J}_\perp^{\,0} - \vec{J}_\perp$ over the layer thickness yields the expression of the electric current per unit length passing within the layer:

$$\vec{I}_{\mathrm{Ha}} = -\int_0^\infty \left(\vec{J}_\perp^{\,0} - \vec{J}_\perp\right) \mathrm{d}N = -\frac{1}{\mathrm{Ha}}\left(\left[\vec{U}_\perp^0\right]_{N=0} \times \vec{y}\right). \tag{13}$$

This relation, which was first established by Hunt and Ludford [4], may also be written $[\vec{U}^0_\perp]_{N=0} = \mathrm{Ha}(\vec{I}_{\mathrm{Ha}} \times \vec{y})$. Is is quite important since it demonstrates that the core velocity is depending on the local current within the layer. More precisely, it shows that, when the Hartmann current is changed (for instance, short-circuited by the wall), the core velocity at any distance from the wall is also changed. As it will be shown in the next section, this condition is particularly crucial when the Hartmann current is of the same order as the core current, i.e., when the current density is Ha times larger in the layer than in the core.

Now, in a way similar to that used to get (11), we may derive from (12) an expression for the component of the current density normal to the wall. However, since the Hartmann wall may have a non zero electric conductivity, the total budget of the electric current perpendicular to the magnetic field must include the wall. The electric current budget writes

$$\left(\vec{\nabla}_\perp \cdot \vec{I}_w\right) - \left(\vec{\nabla}_\perp \cdot \vec{I}_\perp\right) + J^0_{/\!/} = 0. \tag{14}$$

The expressions of the two divergences may be derived from (13) and from the boundary condition derived by Shercliff [9] for thin walls (see also Moreau [7, p. 132]):

$$\left(\vec{\nabla}_\perp \cdot \vec{I}_\perp\right) = \frac{\Omega^0_{/\!/}}{\mathrm{Ha}}, \qquad \left(\vec{\nabla}_\perp \cdot \vec{I}_w\right) = -C \cdot \Delta_\perp \Phi^0, \tag{15}$$

with e, σ_w and $C = \frac{e\sigma_w}{l\sigma}$ the thickness, the electrical conductivity and the conductance ratio of the wall. Thus, Eq. (14) yields the relation valid at the Hartmann wall ($N = 0$):

$$\frac{\partial \Phi^0}{\partial N} = -\frac{\Omega^0_{/\!/}}{\mathrm{Ha}} - C \cdot \Delta_\perp \Phi^0. \tag{16}$$

Together, relations (11), (13) and (16) characterize the specific properties of the Hartmann layer. In the following, we use them as boundary conditions for the core at the Hartmann wall (reducing (11) to its simple form: $U^0_{/\!/(N=0)} = 0$), and we limit ourselves to the case of insulating walls ($C = 0$).

3. Analytical solutions

Our purpose here is to summarize the method in the case where there is no volumetric heat source, so that the temperature is linear in X or Y, and the consequent asymmetry always ensures that the global flow rate is zero. A more complete description is given in Appendix A.

3.1. Core and Hartmann layers

Let us first consider the case of a magnetic field *perpendicular* to the temperature gradient, where $\theta = 1/2 - X$, which illustrates very clearly how the boundary conditions derived above from the Hartmann layer theory determine the velocity and the electric potential within the core. In the core, with Ohm's law (2) and neglecting the Laplacian in Eq. (1), we get

$$J^0_x = -\left(\frac{\partial \Phi^0}{\partial X} + W^0\right) = -\frac{\mathrm{Gr}}{\mathrm{Ha}^2}\theta, \tag{17}$$

whereas, within the Hartmann layers,

$$J_x = J^0_x + \left[W^0\right]_{N=0} \cdot \mathrm{e}^{-\mathrm{Ha}Y}. \tag{18}$$

Integrating Eq. (5) determines the electric potential in the core, with two quantities $A(X)$ and $B(X)$, independent of Y which will soon clearly appear to be respectively linked with the control of the core by the two Hartmann layers and with the core flow rate (the reference for the potential is chosen at the corner of the cross section):

$$\Phi^0 = -\frac{\mathrm{Gr}}{\mathrm{Ha}^2} \int_0^Y \int_0^{Y'} \frac{\partial \theta}{\partial X} \cdot \mathrm{d}Y' \cdot \mathrm{d}Y + Y \cdot A(X) + B(X). \tag{19}$$

Then, from Eq. (17) we get the core velocity

$$W^0 = \frac{\mathrm{Gr}}{\mathrm{Ha}^2}\theta - Y \cdot A'(X) - B'(X). \tag{20}$$

Applying the condition (16) at both insulating Hartmann walls, we get

$$A(X) - \frac{A''(X)}{2\mathrm{Ha}} = \frac{\mathrm{Gr}}{2\mathrm{Ha}^2} \int_0^1 \frac{\partial \theta}{\partial X} \cdot \mathrm{d}Y = -\frac{\mathrm{Gr}}{2\mathrm{Ha}^2}, \tag{21}$$

whose integration yields

$$A(X) = -\frac{\mathrm{Gr}}{2\mathrm{Ha}^2}, \tag{22}$$

and

$$B''(X) = \frac{\mathrm{Gr}}{\mathrm{Ha}^2}\frac{\partial\theta}{\partial X}_{Y=0} - \mathrm{Ha}\cdot A(X) = -\frac{\mathrm{Gr}}{\mathrm{Ha}^2} + \frac{\mathrm{Gr}}{2\mathrm{Ha}}. \tag{23}$$

With no mean flow, and because of the symmetries, the average of the core velocity must be zero:

$$B(X) = \left(\frac{\mathrm{Gr}}{2\mathrm{Ha}} - \frac{\mathrm{Gr}}{\mathrm{Ha}^2}\right)\frac{X^2}{2} - \frac{\mathrm{Gr}}{4\mathrm{Ha}}\left(1 - \frac{2}{\mathrm{Ha}}\right)X. \tag{24}$$

Then we get the following expressions:

$$W^0 = \frac{\mathrm{Gr}}{2\mathrm{Ha}}\theta, \qquad \Phi^0 = -\frac{\mathrm{Gr}}{4\mathrm{Ha}}X(1-X) + \frac{\mathrm{Gr}}{2\mathrm{Ha}^2}\big[X(1-X) - Y(1-Y)\big]. \tag{25}$$

In the case of a magnetic field *parallel* to the temperature gradient ($\theta = 1/2 - Y$), Eqs. (17) and (20) are unchanged, but the electric potential (19) and the boundary conditions at Hartmann walls (21) and (23) are simplified:

$$\Phi^0 = Y\cdot A(X) + B(X) \tag{26}$$

and

$$A(X) - \frac{A''(X)}{2\mathrm{Ha}} = \frac{\mathrm{Gr}}{2\mathrm{Ha}^2}\int_0^1 \frac{\partial\theta}{\partial X}\cdot \mathrm{d}Y = 0, \quad \text{so that } A(X) = 0, \tag{27}$$

$$B''(X) = \frac{\mathrm{Gr}}{\mathrm{Ha}^2}\frac{\partial\theta}{\partial X}_{Y=0} - \mathrm{Ha}\cdot A(X) = 0, \quad \text{so that } B(X) = 0. \tag{28}$$

Finally, in this case where the curl of buoyancy is perpendicular to the magnetic field, the right hand side of Eq. (4) cancels, the Hartmann layers are inactive and

$$W^0 = \frac{\mathrm{Gr}}{\mathrm{Ha}^2}\theta, \qquad \Phi^0 = 0. \tag{29}$$

It is *a posteriori* noticeable that, in the *perpendicular* case, Hartmann layers carry the same electric current as the core ($\approx \mathrm{Gr}/(2\mathrm{Ha}^2)$), whereas in the *parallel* case, the current passing within the Hartmann layer is negligible ($\approx \mathrm{Gr}/\mathrm{Ha}^3$) in comparison with the current passing in half the core. In the *parallel* case, the condition (16) is satisfied since both sides are zero, and, in both configurations, the vertical flow ensures that both terms of condition (11) are zero.

3.2. Side layers

Self-similar solutions may be derived for the side layers along electrically insulating walls. They are equivalent to the Fourier expansion proposed by Bühler [2] in a more general case, but present the advantage to form a class of simple solutions whose integral values have explicit expressions which simplify the calculus of their flow rate. It is necessary when the zero flow rate condition is not automatically satisfied because of the symmetry, or when global flow rate is not zero, as in mixed or forced convection. This analysis relies on the assumption that the values of the core velocity W^0 and of the core electrical current J_x^0 crossing the wall are Y-polynomials at the side wall.

In such a fully-established flow, the electric current circulates in horizontal planes. Let us denote $h(x, y)$ the stream function of the current density, such that $J_x = \partial_y h$ and $J_y = -\partial_x h$ ($\vec{b} = R_m\cdot h\cdot\vec{z}$ is the induced magnetic field, $R_m = \mu\sigma UL = P_m\,\mathrm{Re} \ll 1$ and $P_m = \mu\sigma\nu \sim 10^{-7}$ being the magnetic Reynolds and Prandtl numbers). After substraction of the core solution and reduction of the Laplacian to the derivative normal to the wall, the motion and induction equations become:

$$\frac{1}{\mathrm{Ha}^2}\cdot\frac{\partial^2 W}{\partial X^2} = -\frac{\partial h}{\partial Y}, \qquad \frac{\partial^2 h}{\partial X^2} = -\frac{\partial W}{\partial Y}. \tag{30}$$

Introducing the Elssasser's variables $\nu^+ = W + \mathrm{Ha}\cdot h$ and $\nu^- = W - \mathrm{Ha}\cdot h$, we get parabolic equations similar to the heat equation:

$$\frac{\partial^2\nu^+}{\partial X^2} + \mathrm{Ha}\cdot\frac{\partial\nu^+}{\partial Y} = 0, \qquad \frac{\partial^2\nu^-}{\partial X^2} - \mathrm{Ha}\cdot\frac{\partial\nu^-}{\partial Y} = 0. \tag{31}$$

Table 1
Familly of functions F_n

n	α_n	F_n
0	$-\frac{2}{\sqrt{\pi}}$	$\operatorname{erf} c(\eta)$
1	$-\sqrt{\pi}$	$-\eta\cdot\sqrt{\pi}\operatorname{erf} c(\eta)+\exp(-\eta^2)$
2	$-\frac{4}{\sqrt{\pi}}$	$(1+2\cdot\eta^2)\cdot\operatorname{erf} c(\eta)-\frac{2\cdot\eta}{\sqrt{\pi}}\cdot\exp(-\eta^2)$
3	$-\frac{3}{2\sqrt{\pi}}$	$-\frac{\sqrt{\pi}}{2}(3\cdot\eta+2\cdot\eta^3)\cdot\operatorname{erf} c(\eta)+(1+\eta^2)\cdot\exp(-\eta^2)$
4	$-\frac{16}{3\sqrt{\pi}}$	$(1+4\cdot\eta^2+\frac{4}{3}\cdot\eta^4)\cdot\operatorname{erf} c(\eta)-\frac{2}{3\sqrt{\pi}}\cdot(5\cdot\eta+2\cdot\eta^3)\cdot\exp(-\eta^2)$

The velocity is zero at the walls and the electric condition on the insulating walls imposes the stream function h along the perimeter of the section to be a constant which can be taken as zero. Then, ν^+ and ν^- vanish at the parallel walls. Besides, like the core, the side layers have to satisfy the modified boundary conditions at the Hartmann walls, which are:

$$\left[\frac{\partial\nu^+}{\partial X}\right]_{Y=1}=0,\qquad\left[\frac{\partial\nu^-}{\partial X}\right]_{Y=0}=0. \tag{32}$$

Looking for self-similar solutions for $\nu^+$and ν^-, in the form $\nu=\nu_0(Y)\cdot F(\eta)$, with $F(0)=1$, $F(\infty)=0$, and where $\eta=X/\delta(Y)$ (side layer $X=0$) or $\eta=(1-X)/\delta(Y)$ (side layer $X=1$) denotes the distance to the wall related to the layer's thickness δ, with ν_0 to be determined, we obtain the following equation for $F(\eta)$:

$$F''(\eta)\mp\mathrm{Ha}\cdot\delta(Y)\cdot\delta'(Y)\cdot\left[\eta\cdot F'(\eta)-\frac{\nu_0'(Y)}{\nu_0(Y)}\cdot\frac{\delta(Y)}{\delta'(Y)}\cdot F(\eta)\right]=0. \tag{33}$$

It implies that δ^2 has a linear dependance with Y and that ν_0 is proportional to some power of δ, the exponent being determined by the core solution in order that global Elssasser's variables be zero at the walls. In our case, $\nu^{\pm}(X=0,1)$ are polynomials of Y and may be expressed as $\delta^{2\cdot n}$ (n integer), each term giving its own differential equation because of linearity. Without any more precision on δ and ν_0, this differential equation (with $F_n(0)=1$, and $F_n(\infty)=0$) gives a family of recurrent functions based on $\exp(-\eta^2)$ and $\operatorname{erf} c(\eta)$ (see Moreau [7, p. 138–142] or Hunt and Williams [6]). With such decreasing solutions when $\eta\to\infty$, the boundary conditions become $\delta=0$ at Hartmann walls. Finally we get the expressions

$$\delta^+=\delta_0\cdot\sqrt{1-Y}\quad\text{for }\nu^+,\qquad\delta^-=\delta_0\cdot\sqrt{Y}\quad\text{for }\nu^-. \tag{34}$$

We also take $\nu_0^+(Y)=(1-Y)^{n/2}$, $\nu_0^-(Y)=Y^{n/2}$, and with the choice $\delta_0=1/\sqrt{\mathrm{Ha}}$, we get a family of differential equations for the recurrent functions $F_n(\eta)$:

$$F_n''(\eta)+2\cdot\eta\cdot F_n'(\eta)-2\cdot n\cdot F_n(\eta)=0. \tag{35}$$

The straight forward algebra leading to the solution of this family of functions is given in the appendix, and the first functions ($n\leqslant 4$) are listed on Table 1. Any reader who wants to calculate the electric potential or the flow rate of the layer may find the integration methods in Appendix A.

The main interest of this general technique for the side layers lies in the fact that a small number of terms is sufficient to form the solution of each particular case. It is useful to express the flow rate in terms of the core mean velocity when the lack of antisymmetry makes it non zero, or, in mixed convection, when the global flow rate is non zero. Notice that this solution, valid for insulating or perfect conducting walls, cannot satisfy the conservation of charge at the interface of a wall of finite conductance, since the electric current entering in the wall is a simple derivative of the stream function h, giving Y-terms of maximum power $2n-2$, whereas perpendicular Laplacian of potential is a second derivative of h with X and Y, and gives Y-terms of maximum power $2n-3$.

It is noticeable that this solution exhibits a quite general property of MHD damped flows, where the electric current passing in the side layers is an important characteristic of the damping effect. Whatever the case, the electric current density in the core is order of $\mathrm{Gr}/\mathrm{Ha}^2$. Then the Hartmann current cannot exceed $\mathrm{Gr}/\mathrm{Ha}^2$, and the property (13) implies that the core velocity cannot exceed Gr/Ha. As a consequence, Elssasser's variables are always of order Gr/Ha and the velocity and the current density in side layers are always of order Gr/Ha. In the *parallel* case, where the electric current returns through the core without passing in the Hartmann layers, the damping within the core is strong and the core velocity scales as $(\nu/l)\mathrm{Gr}/\mathrm{Ha}^2$. However, within the boundary layers along the insulating side walls, the current density is almost parallel to the magnetic field, the Lorentz force vanishes and jets develops with high velocities as $(\nu/l)\mathrm{Gr}/\mathrm{Ha}$. These jets carry a flow rate $\mathrm{Ha}^{1/2}$ times larger than the core. In

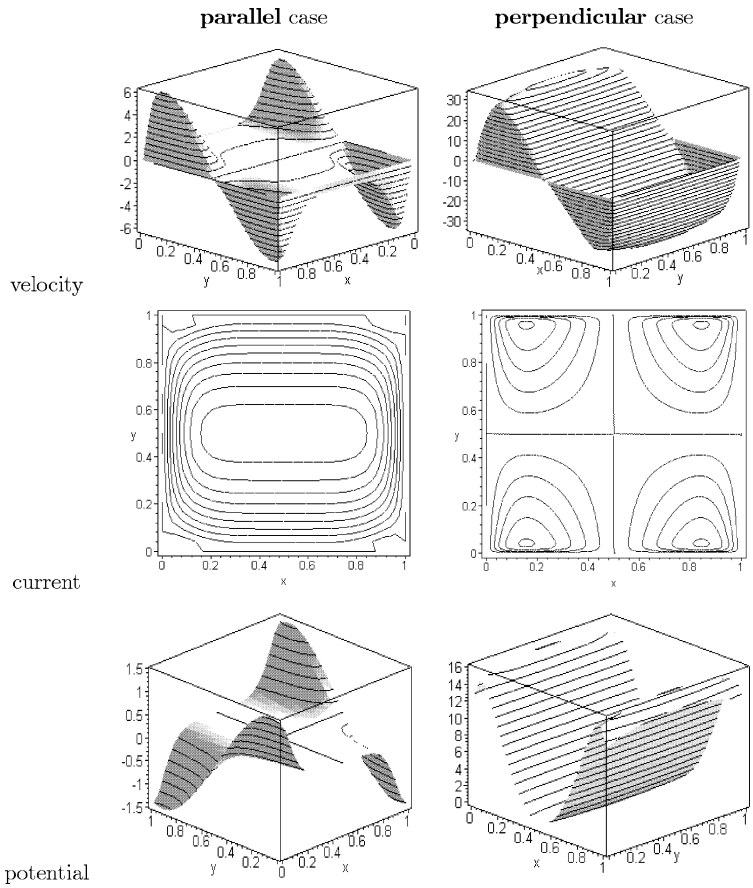

Fig. 3. Analytical results for the parallel and perpendicular cases, with Ha = 100: velocity, electric current streamlines and electric potential.

the *perpendicular* case, the electric current must loop within the Hartmann layers where the local current density becomes Ha times larger than in the core. Then these layers control *via* Eq. (13) the core velocity which scales as $(\nu/l)\mathrm{Gr}/\mathrm{Ha}$ and hide any jet flow in the side layers. Fig. 3 shows in both cases the shapes of the iso-velocity and iso-electric potential lines, as well as the streamlines of the electric current density in the cross section, for Ha = 100. The values of reference are here multiplied by $\mathrm{Gr}/\mathrm{Ha}^2$.

4. Numerical results

This problem has been solved numerically using the finite difference technique HSMAC, developed by Hirt et al. (1972) [3] and previously applied to the case of a cubic enclosure by Tagawa and Ozoe (1997) [12]. In this paper, the HSMAC method was applied for computation of electric current density and electric potential. A fixed and realistic value is chosen for the Gr number ($\mathrm{Gr} = 10^4$), whereas the Ha number is varied. In the following, we present results obtained for Hartmann numbers: 100 (moderate), 500 (intermediate) and 2000 (strong). A time derivative introduced in the momentum equation yields the possibility to use a time marching method and the computations are continued until the results do not change with time. A non-uniform mesh is used, with smaller spacing in the boundary layers than in the center. Our reference grid is composed of 32×32 mesh points (30 internal + 2 external mesh points in each directions), and the coordinates of the 31 points are given in Table 2. One may deduce from these values that there are, respectively, 8, 4, and 2 points within the side layers, when Ha = 100, 500, and 2000. When the boundary conditions for the core and the side layers at the Hartmann walls are derived from Eqs. (10), (11), (13) and (16), this technique is equivalent to the "composite core-side-layer approach" developed by Ting et al. (1993) [13] and Walker and Picologlou (1995) [14]. For example, in this one-dimensional numerical computation, boundary conditions at the Hartmann walls ($Y = 0, 1$) are simplified by using Eqs. (10) and (16) as follows:

Table 2
Grid points

0.000 E+00	1.209 E−02	2.634 E−02	4.305 E−02	6.254 E−02	8.511 E−02
1.111 E−01	1.406 E−01	1.740 E−01	2.112 E−01	2.523 E−01	2.969 E−01
3.446 E−01	3.949 E−01	4.470 E−01	5.000 E−01	5.530 E−01	6.051 E−01
6.554 E−01	7.032 E−01	7.477 E−01	7.888 E−01	8.260 E−01	8.594 E−01
8.889 E−01	9.149 E−01	9.375 E−01	9.570 E−01	9.737 E−01	9.879 E−01
1.000 E+00					

Table 3
Computational parameters and results

	Condition		Without the modelling of the Hartmann layer		With the modelling of the Hartmann layer		Analytical
	Ha	Number of meches	Max. velocity	Velocity gradient	Max. velocity	Velocity gradient	Velocity gradient
Perpendicular case	0	32*32	73.11	373.7	–	–	–
	100	32*32	18.13	58.52	16.43	49.82	50.00
		32*64	16.83	52.09	–	–	
		32*96	16.59	50.99	–	–	
		32*128	16.51	50.66	–	–	
	500	32*32	10.22	31.77	4.073	9.901	10.00
		32*64	6.232	17.23	–	–	
		32*96	5.171	13.55	–	–	
		32*128	4.728	12.10	–	–	
	2000	32*32	–	–	1.123	2.460	2.500
Parallel case	100	32*32	3.059	0.985	2.937	1.006	1.000
	500	32*32	0.713	0.040	0.577	0.040	0.040

$$\frac{\partial W}{\partial Y} = 0 \quad \text{at } Y = 0, 1, \tag{36}$$

$$J_Y = -\frac{1}{\mathrm{Ha}}\frac{\partial W}{\partial X} \quad \text{at } Y = 0, \quad \text{and} \quad J_Y = \frac{1}{\mathrm{Ha}}\frac{\partial W}{\partial X} \quad \text{at } Y = 1. \tag{37}$$

An attempt has also been made to model the Hartmann layer numerically, for the moderate value of Hartmann number (Ha = 100), by increasing the number of mesh points in the direction of the magnetic field, in order to compare the results with those obtained with the analytical modeling of that layer. In this particular case, the number of points in the Hartmann layer is close to 1, 2, 3 and 4, when the number of meshes is 32, 64, 96 and 128, respectively. This test has been repeated for Ha = 500, when the Hartmann layer thickness is always smaller than the smallest mesh spacing. Let us take the velocity gradient at the center of the square for our first comparison for the case of a magnetic field *perpendicular* to the temperature gradient. According to Eq. (25), this quantity should be $-\mathrm{Gr}/(2\mathrm{Ha})$ for $\mathrm{Ha} \gg 1$, i.e., the value is 50, 10, 2.5, respectively, for $\mathrm{Gr} = 10^4$ and Ha = 100, 500, 2000. As shown in Table 3, the values computed with the analytical modelling of the Hartmann layer are nearly equal to these values: 49.82, 9.901, 2.460, even in the case for Ha = 2000. This demonstrates that the results are not very sensitive to the side layers, where no significant electric current is passing. But the values computed without the analytical modeling of the Hartmann layers are far from the asymptotic value in all cases, due to numerical problems.

Fig. 4 shows the velocity distribution in the *perpendicular* case for Ha = 100 and 500, obtained numerically without and with the analytical modelling of the Hartmann layer, in comparison with the analytical asymptotic solution obtained in Section 3. The number of mesh points is 32×32. For Ha = 100, the figures obtained numerically do not seem to reveal a strong difference, but the velocity gradient at the core are respectively 58.52 and 49.82, whereas the asymptotic value is 50. This difference is indeed not small. On the other hand, for Ha = 500, the value of this velocity gradient, derived numerically, are 31.77 and 9.901, whereas the analytical value is 10.

Fig. 5 shows the influence of the number of mesh points within the Hartmann layer when the numerical computation is made without the analytical modelling. The vertical axis shows the ratio between the numerical and the theoretical values of the velocity gradient in the core. When Ha = 100, as the number of mesh points within the Hartmann layer increases, the value tends to unity. But, for Ha = 500, it is quite difficult to obtain reasonable results without using the analytical modeling of the Hartmann layer because of its thinness. As Sterl already observed in 1990 [11], this figure indicates that at least 2 or 3 mesh

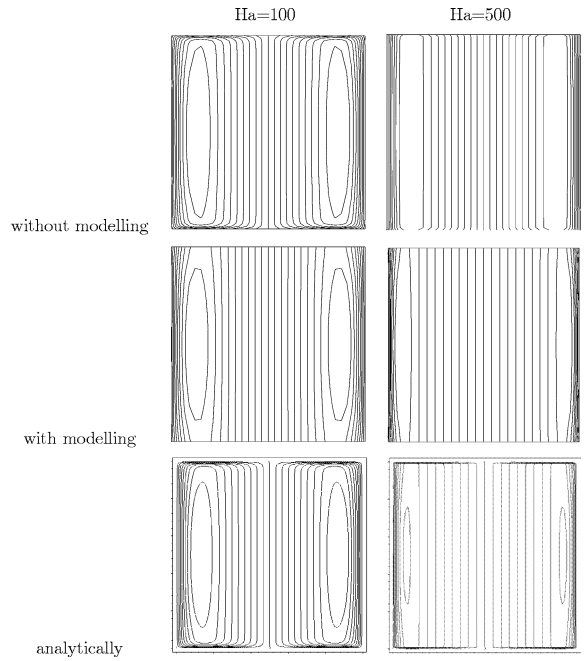

Fig. 4. Comparison of the velocity distributions (iso-velocity lines) obtained with or without the analytical modeling of the Hartmann layer, and with the asymptotic solution.

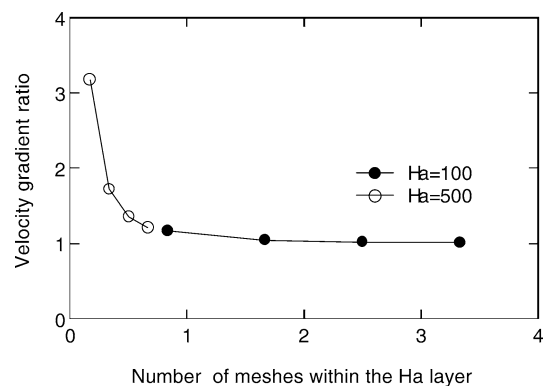

Fig. 5. Influence of the number of meshes in the Ha-layer in the perpendicular case.

points are necessary within the layer. This means that the smallest mesh spacing should be 0.001 for Ha = 500. In other words, it should be necessary to use 1000 mesh points in each direction with a uniform grid, and this is obviously quite impracticable.

In the case of a magnetic field *parallel* to the temperature gradient, similarly, the values of the velocity gradient at the center computed with or without the analytical modeling are both in good agreement with the analytical asymptotic values. This is due to the fact that, in this *parallel* case, there is no electric current in the Hartmann layer.

In Table 3, the values of both the maximum velocity near the hot wall and the velocity gradient at the center in both cases (with and without the analytical modeling of the Hartmann layer) are also compared. Notice that, because of the linear dependence between the velocity and the abscissa (see Eq. (25)), the comparison with the analytical value is only significant when the side layer thickness is very small, i.e., at the high Ha numbers. For Ha = 2000, (strong magnetic field), a fairly good value (1.123 instead of 1.194) is obtained with this analytical modeling and even with the smallest grid (32×32). But for the intermediate and moderate Hartmann numbers, a significant discrepancy is present (4.073 instead of 4.553, 16.43 instead of 20.00). When the maximum velocities computed with and without the analytical modeling of the Hartmann layer are compared to each other, it appears that, if the mesh is not fine enough, the discrepancy may become very large.

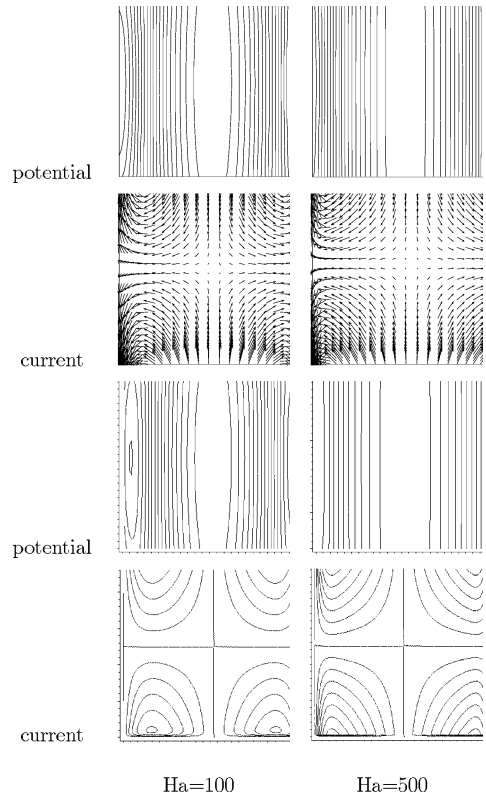

Fig. 6. Contour lines of the potential and current density vectors in the *perpendicular* case, with Ha = 100, 500. Above: numerically with the modelling of the Hartmann layer. Below: analytically. In the case of Ha = 500, the length scale for the current density vectors as been multiplied by a factor 20.

Fig. 6 shows the iso-electric potential lines, and electric current density vectors for the *perpendicular* case, with Ha = 100 and 500. The four figures above have been obtained numerically with the analytical modeling of the Hartmann layer and the four figures below analytically. This figure illustrates, as Fig. 3 (left), the fact that the variations of velocity and potential along the direction of the magnetic field are located in the side layers, and disappear when Ha increases. The next paper Part II will show that they also disappear for a non parallel flow. Then, the flow becomes highly 2D when the Hartmann number is larger than a few hundred (see also Fig. 5). This property might be used to reduce the computational resources for engineering purposes.

Fig. 7 displays the iso-contours of velocity and electric potential, as well as electric current density vectors, for the *parallel* case, when Ha = 100. Those results have been obtained either numerically without (left) the analytical modeling of the Hartmann layer, or analytically (right). Let us notice that the velocity in the core and in the side layers is respectively 50 and 5 times lower than in the *perpendicular* case for the same Hartmann number.

5. Concluding remarks

A buoyant flow in a long vertical enclosure in the presence of a strong horizontal magnetic field is studied numerically with and without the analytical modeling of the Hartmann layer, and the numerical results are compared with analytical asymptotic solutions for Ha $\gg$ 1. In this first paper (Part 1), we limit ourselves to the fully-established buoyant flow, far from the top and the bottom of the enclosure, so that the domain in which the equations are solved numerically and analytically is just the square cross-section. The two most important orientations of the magnetic field (*perpendicular* or *parallel* to the heat flux) are considered.

In the *perpendicular* case, the electric current lines loop within the thin Hartmann layers, which become active, so that the flow is moderately braked and scales as Gr/Ha. In this case, for numerical computations, the use of the analytical modeling of the Hartmann layer seems unavoidable and yields results precisely and quickly without resolving the Hartmann layers numerically. As expected, the variations of the velocity and the electric potential in the direction of the magnetic field disappear with

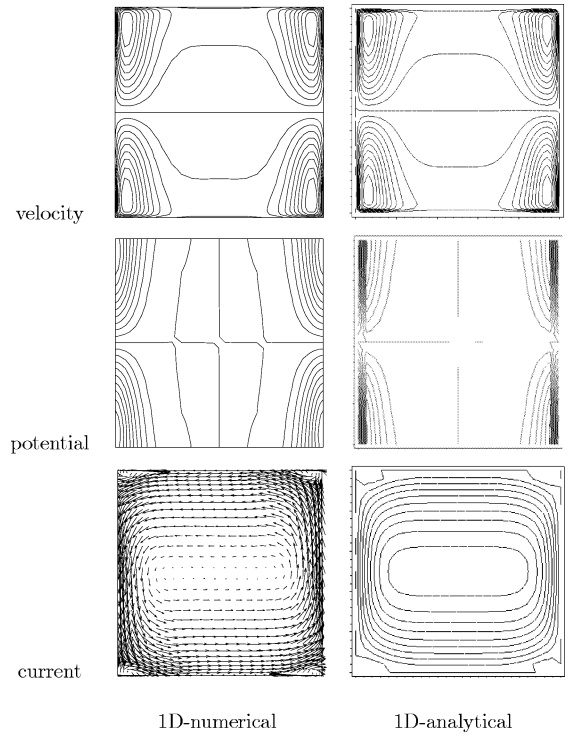

Fig. 7. Contour lines of velocity, potential and current density vectors for Ha = 100 for the *parallel* case.

increasing Hartmann number. So far, the influence of the flow on the temperature distribution is ignored in both *parallel* and *perpendicular* cases. But, especially in this *perpendicular* case because of the high velocities, this convective effects should be taken into account. We need to consider the heat carried by the flow. This will be the purpose of a next paper (Part 2).

In the *parallel* case, the buoyant flow is damped out as $\mathrm{Gr}/\mathrm{Ha}^2$ in the core, since the Hartmann layers are inactive. But the electric current, pushed toward two opposite side walls according to the sign of the velocity, goes along these insulating walls and becomes almost parallel to the magnetic field, so that this damping effect vanishes locally. Two jets of opposite sign appear in each side layer. Their velocity scales as Gr/Ha, and the strong inflection of this velocity profile might excite some instabilities. But, because of the oddness in the X direction, any disturbance cannot be quasi two-dimensional as in duct flows, and should be submitted to a strong Joule damping. This question would deserve some deeper investigations, namely experimental.

Now, the relevance of these solutions for fully-established flows for any practical experiment with a finite enclosure of total height H deserves some discussion. The key point is the change of the temperature distribution due to the convection, which should increase with the ratio between the enthalpy flux convected upwards or downwards in each half cross section $\phi_{\mathrm{conv}} = \iint_{S/2} \rho C_p T w \cdot \mathrm{d}x \cdot \mathrm{d}y$, and the conductive horizontal heat flux from the hot wall to the cold one $\phi_{\mathrm{cond}} = \lambda \cdot \Delta T \cdot H$. A significant approximation of this ratio $\phi_{\mathrm{conv}}/\phi_{\mathrm{cond}}$, commonly called Péclet number, may be derived from the expressions of the core velocity: $\frac{1}{4} \cdot \frac{\mathrm{Pr}\cdot\mathrm{Gr}}{\mathrm{Ha}} \cdot \frac{l}{H}$ in the *perpendicular* case and $\frac{1}{2} \cdot \frac{\mathrm{Pr}\cdot\mathrm{Gr}}{\mathrm{Ha}^2} \cdot \frac{l}{H}$ in the *parallel* case. It is clear that, in both cases, but especially in the *parallel* case which maximizes the damping effect, as soon as Ha is large enough, the convective disturbance of the temperature distribution may be relatively small.

Appendix A

A.1. Calculation of the core flow for any temperature distribution

In the core, neglecting the Laplacian in Eq. (1), we get

$$J_x^0 = -\left(\frac{\partial \Phi^0}{\partial X} + W^0\right) = -\frac{\mathrm{Gr}}{\mathrm{Ha}^2}\theta, \tag{A.1}$$

whereas, within the Hartmann layers,

$$J_x = J_x^0 + \left[W^0\right]_{N=0} \cdot \mathrm{e}^{-\mathrm{Ha}Y}. \tag{A.2}$$

Integrating Eq. (5), we determine the electric potential in the core

$$\Phi^0 = -\frac{\mathrm{Gr}}{\mathrm{Ha}^2} \int_0^Y \int_0^{Y'} \frac{\partial\theta}{\partial X} \cdot \mathrm{d}Y' \cdot \mathrm{d}Y + Y \cdot A(X) + B(X) \tag{A.3}$$

and then we get the core velocity

$$W^0 = \frac{\mathrm{Gr}}{\mathrm{Ha}^2}\left[\theta + \int_0^Y \int_0^{Y'} \frac{\partial^2\theta}{\partial X^2} \cdot \mathrm{d}Y' \cdot \mathrm{d}Y\right] - Y \cdot A'(X) - B'(X). \tag{A.4}$$

With the simplified energy equation $\nabla^2\theta + Q = 0$ (in the limit of pure conductive heat flux), where Q represents a given volumetric heat source, this relation becomes

$$W^0 = \frac{\mathrm{Gr}}{\mathrm{Ha}^2}\left[\theta_{Y=0} + Y \cdot \frac{\partial\theta}{\partial Y}_{Y=0} - \int_0^Y \int_0^{Y'} Q \cdot \mathrm{d}Y' \cdot \mathrm{d}Y\right] - Y \cdot A'(x) - B'(x). \tag{A.5}$$

Applying the condition (16) at both insulating Hartmann walls, we get

$$A(X) - \frac{A''(X)}{2\mathrm{Ha}} = \frac{\mathrm{Gr}}{2\mathrm{Ha}^2} \int_0^1 \frac{\partial\theta}{\partial X} \cdot \mathrm{d}Y - \frac{\mathrm{Gr}}{2\mathrm{Ha}^3} \cdot \left\{\int_0^1 \int_0^Y \frac{\partial^3\theta}{\partial X^3} \cdot \mathrm{d}Y' \cdot \mathrm{d}Y + \left[\frac{\partial\theta}{\partial X}\right]_{Y=0}^{Y=1}\right\}, \tag{A.6}$$

or using the simplified energy equation

$$A(X) - \frac{A''(X)}{2\mathrm{Ha}} = \frac{\mathrm{Gr}}{2\mathrm{Ha}^2} \int_0^1 \frac{\partial\theta}{\partial X} \cdot \mathrm{d}Y + \frac{\mathrm{Gr}}{2\mathrm{Ha}^3} \cdot \left\{\int_0^1 \int_0^Y \frac{\partial Q}{\partial X} \cdot \mathrm{d}Y' \cdot \mathrm{d}Y - \frac{\partial^2\theta}{\partial X \cdot \partial Y}_{Y=0}\right\} \tag{A.7}$$

and

$$B''(X) = \frac{\mathrm{Gr}}{\mathrm{Ha}^2} \frac{\partial\theta}{\partial X}_{Y=0} - \mathrm{Ha} \cdot A(X). \tag{A.8}$$

In the first integration of (A.8), a new constant W_0 has to be introduced which is directly linked with the core velocity via Ohm's law. It can only be adjusted when the side layers (Section 3.2) are taken into account, in such a way to get the expected flow rate. In both *parallel* or *perpendicular* cases, when the volumetric heating is zero, the average core velocity must be zero and condition (A.7) becomes:

$$A(X) = \frac{\mathrm{Gr}}{2\mathrm{Ha}^2} \int_0^1 \frac{\partial\theta}{\partial X} \cdot \mathrm{d}Y. \tag{A.9}$$

A.2. Full description of the side layers

The solution in the side layers is given by the family of functions F_n, which are solutions of the differential equation:

$$F_n''(\eta) + 2 \cdot \eta \cdot F_n'(\eta) - 2 \cdot n \cdot F_n(\eta) = 0. \tag{A.10}$$

Pointing out that $F_n' = F_n'(0) \cdot F_{n-1}$, and $F_0 = \mathrm{erf}\,c(\eta)$, all the set $\{F_n(\eta)\}$ is reached. Denoting $\alpha_n = F_n'(0)$, P_n and Q_n being two polynomials, and A_n being a scalar, it can be demonstrated by recursion that

$$\begin{aligned} &F_n(\eta) = A_n \cdot \left[P_n(\eta) \cdot \exp\left(-\eta^2\right) - \sqrt{\pi} \cdot Q_n(\eta) \cdot \mathrm{erf}\,c(\eta)\right], \\ &\alpha_{2n} = -\frac{4^n n!^2}{(2n)!} \cdot \frac{2}{\sqrt{\pi}}, \qquad A_{2n} = \frac{4^n n!}{(2n)!} \cdot \frac{2}{\sqrt{\pi}}, \qquad \alpha_{2n+1} = -\frac{(2n+1)!}{4^n n!^2} \cdot \sqrt{\pi}, \qquad A_{2n+1} = \frac{1}{n!}, \end{aligned} \tag{A.11}$$

where P_n and Q_n are obtained from the same recursive relation, but with different initial conditions:

$$P_n(\eta) = \frac{n-1}{2} P_{n-2}(\eta) - \eta \cdot P_{n-1}(\eta), \qquad P_0 = 0, \qquad P_1 = +1,$$
$$Q_n(\eta) = \frac{n-1}{2} Q_{n-2}(\eta) - \eta \cdot Q_{n-1}(\eta), \qquad Q_0 = -1, \qquad Q_1 = \eta. \tag{A.12}$$

The solution for both polynomials is build with the matrix T_n,

$$\begin{pmatrix} P_{2n+1}, & Q_{2n+1} \\ P_{2n}, & Q_{2n} \end{pmatrix} = T_n \cdot T_{n-1} \cdots T_1 \begin{pmatrix} 1, & \eta \\ 0, & -1 \end{pmatrix} \quad \text{with } T_n = \begin{bmatrix} n+\eta^2 & -\left(\dfrac{n-1}{2}\right)\eta \\ -\eta & \left(\dfrac{n-1}{2}\right) \end{bmatrix}.$$

Table 1 shows theses functions for $n \leqslant 4$, what is sufficient for both cases where the temperature gradient is uniform, *parallel* or *perpendicular* to the magnetic field. Let us recall that only even terms interest us for Elssasser's variables, we call $E_n^{\pm}$ their coefficients, so that

$$v^+ = \sum_{n \geqslant 0} E_n^+ \cdot (1-Y)^n \cdot F_{2n}(\eta^+), \qquad v^- = \sum_{n \geqslant 0} E_n^- \cdot Y^n \cdot F_{2n}(\eta^-). \tag{A.13}$$

Nevertheless, the odd cases are useful to get some integral values, as in the calculation of the flow rate and of electric potential.

A.2.1. Some integrations…

For calculation of both the flow rate and the electric potential, we need to get the expressions of the two following integrals:

$$I_n(\eta) = \int_{\eta}^{\infty} \frac{F_n(\eta')}{\eta'^{n+3}}\,\mathrm{d}\eta', \qquad H_n(X,Y) = \int_{1/2}^{Y} Y'^{n/2} \cdot F_n\big(\eta^-(X,Y')\big) \cdot \mathrm{d}Y'. \tag{A.14}$$

A by parts integration of the first one leads to the relation of recursion

$$I_n(\eta) = \frac{F_n(\eta)}{(n+2)\eta^{n+2}} + \frac{\alpha_n}{n+2} I_{n-1}(\eta) \tag{A.15}$$

and with the conventions $\prod_{j=n+1}^{j=n} = 1$, and $F_{-1} = F_0'(\eta)/\alpha_0 = \mathrm{e}^{-\eta^2}$, the integral can be expressed by:

$$I_n(\eta) = \sum_{i=-1}^{i=n} \left[\frac{F_i(\eta)}{(i+2)\eta^{i+2}} \cdot \prod_{j=i+1}^{j=n} \frac{\alpha_j}{j+2} \right] - \sqrt{\pi}\,\mathrm{erf}\,c(\eta) \prod_{j=0}^{j=n} \frac{\alpha_j}{j+2}. \tag{A.16}$$

Then we can get

$$H_n(X,Y) = 2\left(\frac{X}{\delta_0}\right)^{n+2} \cdot \big[I_n(\eta^-_{(X,Y)}) - I_n(\eta^-_{(X,1/2)}) \big]. \tag{A.17}$$

A.2.2. Calculation of the flow rate

The calculation of the flow rate within the side layer close to $X = 0$ needs the bi-integration of each Elssasser's variable. We denote

$$D_n^s = \iint\limits_{\substack{\text{cross} \\ \text{section}}} Y^{n/2} \cdot F_n(\eta^-) \cdot \mathrm{d}X \cdot \mathrm{d}Y = \iint\limits_{\substack{\text{cross} \\ \text{section}}} (1-Y)^{n/2} \cdot F_n(\eta^+) \cdot \mathrm{d}X \cdot \mathrm{d}Y.$$

We first integrate F_n along X with the new variable η^- (Y constant) and using the relation $F_n(\eta) = F_{n+1}'(\eta)/\alpha_{n+1}$:

$$\int_{X=0}^{X=1} F_n(\eta^-)\,\mathrm{d}X = -\frac{\delta^-(Y)}{\alpha_{n+1}} \cdot \left[1 - F_{n+1}\left(\frac{1}{\delta^-(Y)} \right) \right]. \tag{A.18}$$

Then, the integration along X leads without difficulties to (remember that α_{n+1} is negative):

$$D_n^s = -\frac{1}{\alpha_{n+1}\sqrt{\mathrm{Ha}}} \cdot \big[1 - 2 \cdot \mathrm{Ha}^{(n+3)/2} \cdot I_{n+1}\big(\sqrt{\mathrm{Ha}}\big) \big]. \tag{A.19}$$

We must add a correction due to the junction of the side and the Hartmann layer. The exponential Hartmann profile makes easy the integration:

$$D_n^{sh} = \iint\limits_{\substack{\text{cross}\\ \text{section}}} \left[Y^{n/2}\cdot F_n(\eta^-)\right]_{Y=1}\cdot \mathrm{e}^{\mathrm{Ha}(Y-1)}\cdot \mathrm{d}X\cdot \mathrm{d}Y = \frac{1-\mathrm{e}^{-\mathrm{Ha}}}{\alpha_{n+1}\cdot \mathrm{Ha}^{3/2}}\cdot\left[1-F_{n+1}\left(\sqrt{\mathrm{Ha}}\right)\right]. \tag{A.20}$$

Finally, we get the flow rate of one side layer, and the global flow rate of the cell:

$$D^s = \sum_{n\geqslant 0}\frac{E_n^+ + E_n^-}{2}\cdot\left[D_n^s + D_n^{sh}\right], \quad \text{and} \quad D = D^c + D^{s+} + D^{s-}. \tag{A.21}$$

A.2.3. Simple equivalents for $\mathrm{Ha}\to\infty$

A change of variable in the integral definition of the $\operatorname{erf} c$ function and four by part integrations lead to the following development:

$$\operatorname{erf} c(\eta) \underset{\eta\to\infty}{\sim} \frac{1}{\eta\cdot\sqrt{\pi}}\cdot\exp\left(-\eta^2\right)\cdot\left(1-\frac{1}{2\eta^2}\right). \tag{A.22}$$

Then, the terms of maximum order in P_n and Q_n cancel each other out in F_n and without calculating the coefficient B_n, we can write a simple equivalent of F_n and of I_n:

$$F_n(\eta) \underset{\eta\to\infty}{\sim} B_n\cdot\eta^{n-3}\cdot\exp\left(-\eta^2\right) \quad \text{and} \quad I_n(\eta) \underset{\eta\to\infty}{\sim} -\frac{\exp(-\eta^2)}{\eta}\cdot\prod_{j=0}^{j=n}\frac{\alpha_j}{j+2}. \tag{A.23}$$

As a result, the term comprising $I_{n+1}(\sqrt{\mathrm{Ha}})$ in D_n^s is negligeable and we have the equivalent

$$D_n^s \underset{\mathrm{Ha}\to\infty}{\sim} -\frac{1}{\alpha_{n+1}\sqrt{\mathrm{Ha}}}, \tag{A.24}$$

which is Ha times larger than the contribution of each composite Hartmann-side layer, $D_n^{sh} \sim_{\mathrm{Ha}\to\infty} \frac{1}{\alpha_{n+1}\cdot\mathrm{Ha}^{3/2}}$. Finally, the flow rate of the side layer is

$$D^s = -\frac{1}{\sqrt{\mathrm{Ha}}}\sum_{n\geqslant 0}\frac{E_n^+ + E_n^-}{2\cdot\alpha_{n+1}}. \tag{A.25}$$

A.2.4. Calculation of the electric potential

The potential is generally given by

$$\Phi(X,Y) = \frac{\partial}{\partial X}\left(\int_{1/2}^{Y} h\cdot\mathrm{d}Y\right) - \int_{1/2}^{Y}\left(V+\frac{\partial h}{\partial Y}\right)_{(X,1/2)}\cdot\mathrm{d}X. \tag{A.26}$$

For the contribution of the side layer, where V and h are given by the Elssasser's variables, we first need to calculate the following expressions:

$$K_n^-(X,Y) = \frac{\partial}{\partial X}\left(\int_{1/2}^{Y} Y'^{n/2}\cdot F_n(\eta^-)\cdot\mathrm{d}Y'\right) = \frac{\partial H_n}{\partial X} = \alpha_n\cdot\sqrt{\mathrm{Ha}}\cdot H_{n-1}(X,Y), \tag{A.27}$$

$$M_n^-(X) = \int_{1/2}^{X}\left[Y^{n/2}\cdot F_n(\eta^-)\right]_{(X',1/2)}\cdot\mathrm{d}X' = \frac{\left[F_{n+1}(\eta^-)\right]_{\eta^-(1/2,1/2)}^{\eta^-(X,1/2)}}{\alpha_{n+1}2^{n/2+1}\sqrt{\mathrm{Ha}}}, \tag{A.28}$$

$$N_n^-(X) = \int_{1/2}^{X}\frac{\partial}{\partial Y}\left[Y^{n/2}\cdot F_n(\eta^-)\right]_{(X',1/2)}\cdot\mathrm{d}X' = \frac{1}{\sqrt{\mathrm{Ha}}\cdot 2^{(n+1)/2}}\cdot\left[(n+1)\frac{F_{n+1}(\eta^-)}{\alpha_{n+1}} - \eta^-\cdot F_n(\eta^-)\right]_{\eta^-(1/2,1/2)}^{\eta^-(X,1/2)} \tag{A.29}$$

and for ν^-, with analog definitions, $K_n^+(X,Y) = -K_n^-(X,-Y)$, $M_n^+(X) = M_n^-(X)$, $N_n^+(X) = -N_n^-(X)$. Thus, we get the potential:

$$\Phi(X,Y) = \frac{1}{2\mathrm{Ha}} \sum_{n\geqslant 0} \left\{ \left(E_n^+ + E_n^-\right) \cdot \left[\mathrm{Ha} \cdot M_n^-(X) - N_n^-(X)\right] - \left[E_n^- \cdot K_n^-(X,Y) + E_n^+ \cdot K_n^-(X,-Y)\right] \right\}. \tag{A.30}$$

The velocity following a possible parity of the temperature, we have if the temperature is even, $E_n^+ = E_n^-$, and if it is odd, $E_n^+ = -E_n^-$. Thus, this potential simplifies as follows:

T even:

$$\Phi(X,Y) = \frac{1}{2\mathrm{Ha}} \sum_{n\geqslant 0} E_n^+ \left\{ 2\left[\mathrm{Ha} \cdot M_n^-(X) - N_n^-(X)\right] - \left[K_n^-(X,Y) + K_n^-(X,-Y)\right] \right\}; \tag{A.31}$$

T odd:

$$\Phi(X,Y) = \frac{1}{2\mathrm{Ha}} \sum_{n\geqslant 0} E_n^+ \left(K_n^-(X,Y) - K_n^-(X,-Y)\right). \tag{A.32}$$

And for the side layer $X \sim 1$, $K_n^{\pm}(X,Y)$, $M_n^{\pm}(X)$, $N_n^{\pm}(X)$ must be respectively replaced by $-K_n^{\pm}(1-X,Y)$, $-M_n^{\pm}(1-X)$, $-N_n^{\pm}(1-X)$ (careful to the fact that the coefficients $E_n^{\pm}$ may have changed).

References

[1] T. Alboussière, J.P. Garandet, R. Moreau, Asymptotic analysis and symetry in MHD convection, Phys. Fluids 8 (1996).
[2] L. Bühler, Laminar buoyant magnetohydrodynamic flow in vertical rectangular ducts, Phys. Fluids 10 (January, 1998) 223–236.
[3] C.W. Hirt, J. Cook, Calculating three-dimensional flows around structures and over rough terrain, J. Comput. Phys. 10 (1972) 324–340.
[4] J.C.R. Hunt, G.S.S. Ludford, Three-dimensional MHD duct flows with strong transverse magnetic fields. Part 1. Obstacles in a constant area channel, J. Fluid Mech. 33 (1968) 693–714.
[5] J.C.R. Hunt, J.A. Shercliff, Annu. Rev. Fluid Mech. (1971) 37.
[6] J.C.R. Hunt, W.E. Williams, Some electrically driven flows in magnetohydrodynamics. Part 1. Theory, J. Fluid Mech. 31 (1968) 705–722.
[7] R. Moreau, Magnetohydrodynamics, Kluwer, 1990.
[8] C.C. Sellers, J.S. Walker, Liquid-metal flow in an electrically insulated rectangular duct with a non-uniform magnetic field, Internat. J. Engrg. Sci. 37 (1999) 541–552.
[9] J.A. Shercliff, The flow of conducting fluids in circular pipes under transverse magnetic fields, J. Fluid Mech. 1 (1956) 644–666.
[10] J. Sommeria, R. Moreau, Why, how, and when, MHD turbulence becomes two-dimensional, J. Fluid Mech. 118 (1982) 507–518.
[11] A. Sterl, Numerical simulation of liquid-metal MHD flows in rectangular ducts, J. Fluid Mech. 216 (1990) 161–191.
[12] T. Tagawa, H. Ozoe, Enhancement heat of heat transfer rate by application of a static magnetic field during natural convection of liquid metal in a cube, J. Heat Transf. 119 (2) (May, 1997) 265–271.
[13] A. Ting, T.Q. Hua, J.S. Walker, B.F. Picologlou, Liquid-metal flow in a rectangular duct with thin metal walls and with a non-uniform magnetic field, Internat. J. Engrg. Sci. 31 (March, 1993) 357–372.
[14] J.S. Walker, B.F. Picologlou, Liquid-metal flow in an insulated rectangular expansion with a strong transverse magnetic field, J. Fluid Mech. 305 (1995) 111–126.